Experimental Validation of Imposed Safety Regions for Neural Controlled Human Patient Self-Feeding using the Modular Prosthetic Limb

Brock A. Wester, Matthew P. Para, Ashok Sivakumar, Michael D. Kutzer, Kapil D. Katyal, Alan D. Ravitz, James D. Beaty, Michael P. McLoughlin, and Matthew S. Johannes*

Abstract— This paper presents the experimental validation of software-based safety features implemented during the control of a prosthetic limb in self-feeding tasks with a human patient. To ensure safe operation during patient controlled movements of the limb, velocity-based virtual fixtures are constructed with respect to the patient's location and orientation relative to the limb. These imposed virtual fixtures or safety zones modulate the allowable movement direction and speed of the limb to ensure patient safety during commanded limb trajectories directed toward the patient's body or environmental obstacles. In this implementation, the Modular Prosthetic Limb (MPL) will be controlled by a quadriplegic patient using implanted intracortical electrodes. These virtual fixtures leverage existing sensors internal to the MPL and operate in conjunction with the existing limb control. Validation of the virtual fixtures was conducted by executing a recorded set of limb control inputs while collecting both direct feedback from the limb sensors and ground truth measurements of the limb configuration using a Vicon tracking system. Analysis of the collected data indicates that the system performed within the limitations prescribed by the imposed virtual fixtures. This successful implementation and validation enabled the approved clinical use of the MPL system for a neural controlled self-feeding task.

Index Terms— Prosthetics, virtual fixtures, teleoperation, motion tracking, patient safety, self-feeding, brain computer interface, neural prosthetic system, cortical control

I. INTRODUCTION AND BACKGROUND

The hybridization, cooperation, and synergy of man with machine continues to fascinate and drive technological advancement on a number of research fronts. These systems are often referred to as Neural Prosthetic Systems (NPS), Neural Interface (NI) systems, Brain Machine Interface (BMI) systems, Brain Computer Interfaces (BCI), or Neuromotor Protheses (NMP), and involve technological advancements and collaborations in robotics, neuroscience, computer science, materials science, and signal processing. Effector devices such as neural-directed prosthetics and robotic assistive devices seek to restore lost function to users such as amputees and persons with debilitating neuromuscular

Fig. 1. The Modular Prosthetic Limb (MPL) developed by the Johns Hopkins University Applied Physics Laboratory as part of the Revolutionizing Prosthetics program.

conditions [1]–[3]. These devices are typically designed to look, feel, weigh, and perform in a capacity commensurate with their human analog and serve to restore lost function to the user, specifically in performing Activities of Daily Living (ADLs). One such activity that currently requires assistive care but could be performed by an NPS is the act of feeding oneself.

A. The Modular Prosthetic Limb

The MPL (Fig. 1) is an advanced upper-extremity prosthetic and human rehabilitation device [4]. From weight and volumetric envelope to speed, torque, and range of motion, the MPL is designed specifically to mimic the capabilities, form factor, and function of the human arm and hand. The upper arm consists of three segments that comprise a shoulder with two drives (abduction/adduction and flex/extend), a humeral rotator, and an elbow with an attached forearm containing an integrated battery compartment. A wrist segment with three drives (rotation, flexion, and deviation) mounts to this as does a hand with independently articulating fingers. With the central software control system (Limb Controller (LC)) [5] present within the palm, the MPL can function with any combination of segments proximal to the hand to accommodate a wide range of amputee residual limb lengths. As part of a strategy to maximize dexterity, speed, and torque generation given the 50th percentile military male design envelopes for weight and volume, the MPL has 17 controllable DOF and 26 articulating DOF in total. The large number of articulating DOF compared to the controllable DOF, specifically within the fingers of the hand, is accomplished primarily through coupled kinematics and differential linkages. Other advanced prosthetic devices with
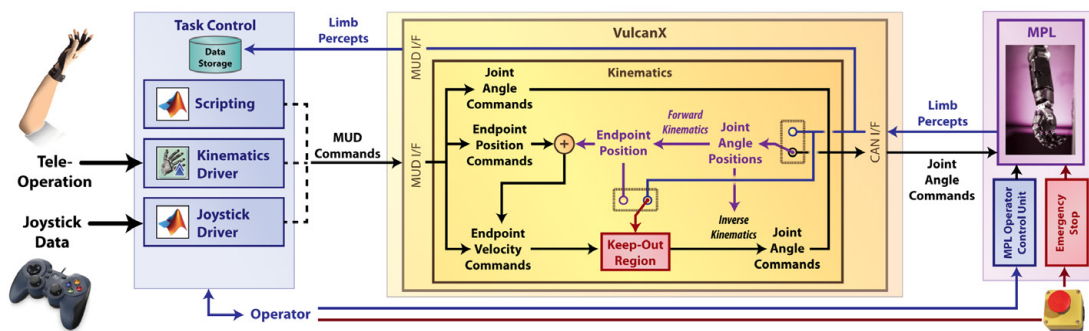
Fig. 2. High-level block diagram presenting an overview of the experimental system with pre-programmed script (MATLAB), joystick (Logitech Gamepad F310), and teleoperation (Cyberglove Systems and Microstrain GX3 inertial sensors) based command inputs.

hand-like effectors (e.g., the DEKA Gen 3 arm, the BeBionic Hand, the iLimb Ultra, and the Michaelangelo hand) are extremely capable prosthetic devices designed to increase user acceptance and functionality in performing ADLs. However, these end-effectors have less dexterity from fewer upper arm joints, reduced sensorization for user feedback, and potentially limited or no modular segmentation to permit use by a wide range of patient populations. Some robotic manipulation systems, or arms on humanoid robots, are able to meet the dexterity of the MPL (e.g., DLR Light-Weight Robot (LWR) III, DLR Hand Arm System, Honda Asimo, HRP, Robonaut), but fail to meet key requirements for patient acceptance such as size, weight, and anthropomorphic form factor. Outside the scope of this document is a review of these different types of human-like manipulation system [6].

B. Clinical MPL Integration

The DARPA Revolutionizing Prosthetics (RP3) program is focused on leveraging advanced neural implant technologies to enable human based closed loop cortical control of the MPL [7]. The term 'closed loop' in this context describes a control paradigm that begins with decoded command inputs derived from direct neural cortical sensing, MPL interaction with and sensing of a target objects, and the resulting cortical feedback of afferents through sensory mapping and neural implant stimulation. RP clinical trials involving the MPL have redefined the degree of control NPSs can achieve, with reported 7-DOF control of the MPL end-effector position/orientation and grasp configuration (6-DOF endpoint position and orientation with 1-DOF grasp control) [8]. Given this success in control and the anthropomorphic form and function of the MPL, the NPS was uniquely qualified for testing of ADL-related tasks. Institutional Review Board (IRB) approval is a requirement with any experimental protocol involving human subjects. For the MPL to operate in close proximity to a patient during these self-feeding experiments, the IRB requires supporting data showing that safety mechanisms are in place to prevent patient injury. These safety mechanisms were required to be implemented along with current limiting of joint actuators, continuously monitored emergency stops, and configurable joint velocity limits. This report presents the methods and results of experimentation conducted to verify a series of

clinical user tunable keep-out and reduced-velocity regions to safely limit the operation of the MPL in close proximity to a patient. With these safety measures in place, the patient was able to perform a self-feeding task using the 7-DoF control of the MPL [9] (supplementary video). For this report we leverage prior work in the area of virtual fixtures, which are commonly used in teleoperated robotic systems with haptic feedback to the operator [10]–[13]. The central theme in many of these past approaches is rooted in the master-slave relationship between control device and robotic manipulator and the bilateral force reflectivity between them [14] (and others). This type of approach can be especially useful for robotic-assisted surgical systems, which employ similar approaches sometimes referred to as 'no-fly zones' [15]–[20]. These virtual fixtures serve to prevent unwanted motion of the robotic end-effector(s) into specific regions of the configuration space and indicate these restrictions to the operator through haptic or visual feedback. Forbidden Region Virtual Fixtures (FRVFs), specific nomenclature for these types of approaches, have been applied in a variety of use cases and have been extensively developed with varying methods of implementation [13], [21]. For this effort, the specific focus is to prevent/limit the end-effector motion within specific regions of the MPL workspace as well as to apply corrective velocity of the effector away from these defined boundaries.

II. METHODS

A. System Overview and MPL Kinematics

The MPL control system is comprised of discrete subsystems (Fig. 2). Input commands to the system from sources such as teleoperation devices and control scripts are funneled through a software front-end called VulcanX, which adheres to a defined User Datagram Protocol (UDP)-based communication interface. VulcanX contains the front-end UDP input/output (I/O) communication protocol definitions, the back-end MPL Controller Area Network (CAN) I/O communication protocols, and runs the overall control framework. Specifically, the control framework in this experiment handles the MPL forward kinematics, inverse kinematics, and virtual fixtures. The clinical practitioner can define the geometric dimensions of the velocity zones and ultimate keep
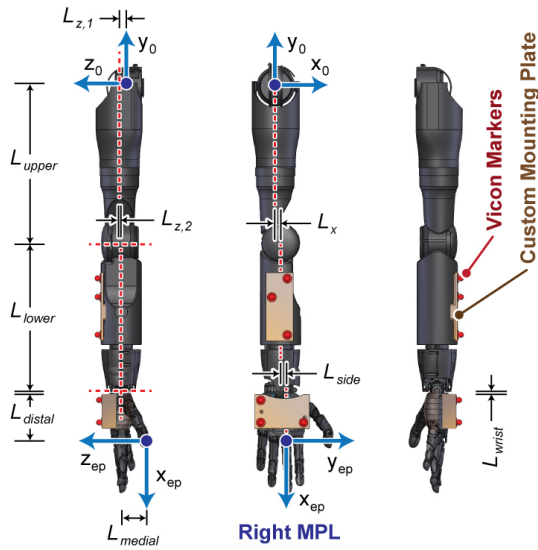
Fig. 3. MPL system geometry and coordinate frame assignments for the upper arm and the wrist.

TABLE I

D-H PARAMETERS FOR MPL WHERE $L_{z,1}$ = -13.89, $L_{z,2}$ = -3.12, L_x = -10.00, L_{upper} = -288.70, L_{lower} = -268.70, L_{wrist} = 7.00, L_{distal} = 84.60, L_{medial} = 46.12, AND L_{side} = 10.00 mm.

Link i	a_i	α_i	d_i	θ_i	$[\theta_{i,min}, \theta_{i,max}]$
1	0	-90°	0	-90 + θ_1	[-40°, 175°]
2	$L_{z,1}$	-90°	0	90 + θ_2	[-160°, 20°]
3	L_x	90°	L_{upper}	-90 + θ_3	[-45°, 90°]
4	0	-90°	$L_{z,2}$	θ_4	[0°, 150°]
5	0	-90°	L_{lower}	θ_5	[-90°, 90°]
6	L_{wrist}	90°	0	90 + θ_6	[-45°, 45°]
7	L_{distal}	-90°	0	θ_7	[-60°, 60°]
8	L_{side}	180°	L_{medial}	-90°	
9	0	0°	0	-90°	

out regions in an editable text configuration file.

The MPL system is comprised of a distributed control architecture commanded by the LC with 17 individual motor controllers at each controllable DOF. For the scope of this report, we are primarily concerned with joints 1-7, which correspond to the 4 joints of the upper arm and 3 joints of the wrist as shown in Fig. 3. The range of motion for each of these joints is summarized in Table I.

1) Forward Kinematics: The forward kinematics of the MPL system are calculated based upon the information in Fig. 3 and established methods. The forward kinematics from the shoulder to the endpoint, H_9^0, for a right handed MPL system are defined as:

$$H_9^0 = Z_{d_0,\theta_0} X_{a_0,\alpha_0} Z_{d_1,\theta_1} X_{a_1,\alpha_1} \cdots Z_{d_n,\theta_n} X_{a_n,\alpha_n} \quad (1)$$

where $n \in \{0, 1, \ldots, 9\}$, $Z_{d,\theta}$ and $X_{a,\alpha}$ are represented by the standard Denavit-Hartenberg (D-H) transformation matrices about the relative z and x axes:

$$Z_{d,\theta} = R_{z,\theta} T_{z,d} \quad and \quad X_{a,\alpha} = T_{x,a} R_{x,\alpha} \quad (2)$$

2) Endpoint Control: The limb system is capable of receiving Cartesian endpoint commands, and controlling the upper arm and wrist joints in a coordinated fashion to make the hand move to the position specified. The endpoint control scheme can be fundamentally described as a simple resolved rate control algorithm leveraging the damped pseudo-inverse of the Jacobian.

Given the forward kinematics described in (1) and defining $\vec{q} = (\theta_1, \theta_2, \theta_3, \ldots, \theta_7)^\mathsf{T}$, the mapping between joint angles $(\vec{q})$ and the endpoint position $(\vec{x} = (x, y, z)^\mathsf{T})$ is easily calculated. Representing this as $h(\circ)$ yields

$$\vec{x} = h(\vec{q}) \quad (3)$$

From this, the relationship between endpoint and joint velocities and vice versa can be defined using the Jacobian $(J(\vec{q}))$ as follows

$$\dot{\vec{x}} = J(\vec{q})\dot{\vec{q}} \quad (4)$$

$$\dot{\vec{q}} = J(\vec{q})^\dagger \dot{\vec{x}} \quad (5)$$

where $(\circ)^\dagger$ represents the Moore-Penrose pseudoinverse. Recall that the elements of the Jacobian $(J(\vec{q}))$ are defined as

$$J_{i,j}(\vec{q}) = \frac{\partial h_i(\vec{q})}{\partial q_j} \quad (6)$$

where in this case, $i \in \{1, 2, 3\}$, $j \in \{1, 2, \ldots, 7\}$, and $h_i(\vec{q})$ and q_j represent the *ith* element of the endpoint position and *jth* element of the vector of joint angles, respectively.

Following (5), given a desired endpoint $\vec{x}^*$, and a measurement of the current manipulator configuration $\vec{q}(t_i)$, generic iterative method is adopted to calculate the desired endpoint velocity $(\vec{V}_{cmd})$ and joint velocities required to move to a desired endpoint in the absence of singularities based upon a velocity conversion (k_v) that is a function of desired performance and the time step.

$$\vec{V}_{cmd} = k_v \left(\vec{x}^* - h(\vec{q}(t_i)) \right) \quad (7)$$

and

$$\dot{\vec{q}}(t_{i+1}) = J(\vec{q}(t_i))^\dagger \vec{V}_{cmd} \quad (8)$$

For the case where $J(\vec{q})J(\vec{q})^\mathsf{T}$ loses rank, the Moore-Penrose pseudoinverse is replaced with the damped pseudoinverse $(\circ)^\ddagger$ where

$$J(\vec{q}(t_i))^\ddagger = J(\vec{q}(t_i))^\mathsf{T} \left(J(\vec{q}(t_i))J(\vec{q}(t_i))^\mathsf{T} + \lambda^2 I \right)^{-1} \quad (9)$$

and $\lambda > 0$ is introduced to avoid inverting a singular matrix.

B. Onboard Sensor Overview

The Large Motor Controllers (LMCs) for each of the upper arm drives consist of two sensory methods used for position measurement. The output of the drive contains a sine/cosine encoder used for absolute position sensing and provides an analog signal that is digitized by the microcontroller's 12-bit Analog to Digital Converter (ADC). Because of non-linearity associated with this sensor, a 64 element lookup table is used to map raw ADC values to joint angles in
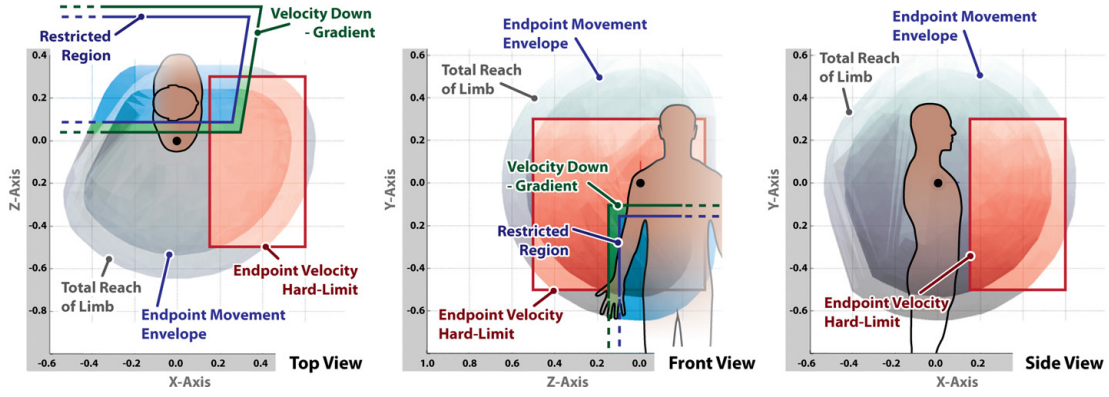
Fig. 4. Depiction of the implemented virtual fixtures, clearly shown in the ultimate endpoint workspace (red), the MPL total movement envelope (gray volume), and the clinical user definable FRVFs (blue and green in the front and top views).

radians with linear interpolation used for values between the look up table indices. At the motor level, two Hall effect sensors are also used to provide relative motor position. These sensors provide 96 counts per electrical revolution and are used for motor commutation. In spite of this sensor's high resolution, because it is located at the motor level (prior to the gear train) it is difficult to use for absolute position sensing due to backlash in the gear train in addition to any mechanical slipping that may be caused by sudden changes in drive velocity. Note that very slight slipping due to high velocity changes in direction happens at frictional gear train elements connected to the motor rotor that exist to reduce operational noise. For this reason, the absolute position derived from the motor position angle is compared to the sine/cosine encoder's absolute position sensor at a rate of 500 Hz. This is adjusted at a maximum rate of $1°/s$ to compensate for any slipping in the drive. In practical use, a prosthetic user can compensate for any errors in sensor alignment using visual feedback and control commands.

C. Imposing Keepout Regions

Multiple virtual fixtures are defined to limit the traversable space of the MPL's endpoint. The primary fixture is imposed to keep the endpoint within a user configurable volume. This is defined as a rectangular solid oriented with the shoulder reference frame (Frame-0, Fig. 3), with minimum and maximum values defining the boundaries of the volume along all three axes of the shoulder frame. The volume associated with the primary fixtures is highlighted red in Fig. 4.

Secondary FRVFs were added over time to block out additional areas within the workspace from the limb. These regions are used to protect a patient who may be positioned very close to the limb from inadvertently causing the limb to collide with themselves, their chair/wheelchair, or the stand used to mount the limb. These additional regions are defined in a similar fashion to the primary virtual fixture, and likewise are easily customizable by the clinician. Representations of secondary fixtures are indicated by the green and blue boundaries in Fig. 4.

The control algorithm monitors the current endpoint of the limb and then loops through all planar elements of the safety regions. If it determines that the endpoint is within a configurable safety distance to any of these virtual fixtures, the algorithm will begin to reduce the commanded endpoint velocity in the normal direction toward the planar elements of the FRVFs defined by the unit vector $\hat{v}_{pb}(\vec{q})$ illustrated in Fig. 5. The user's desired velocity ($\vec{V}_{des}$) in Cartesian space is reduced by two factors, a 'pushback' velocity ($\vec{V}_{pb}$) and a slowdown velocity ($\vec{V}_s$), which are defined as a function of the prescribed minimum safety distance (d^*), the critical minimum safety distance (d_c^*), and the distance to the plane ($d(\vec{q})$). d^* and d_c^* are sometimes referred to as a 'distance of influence' [22]:

$$\vec{V}_s = -\alpha \left(1 - \sqrt{\frac{d(\vec{q})}{d^*}} \right) \hat{v}_{pb} \qquad (10)$$

$$\vec{V}_{pb} = -\left(\frac{d_c^* - d(\vec{q})}{d_c^*} \right)^2 \hat{v}_{pb} \qquad (11)$$

$$\vec{V}_{cmd} = \begin{cases} \vec{V}_{des} + \vec{V}_s + \vec{V}_{pb} & \forall \ 0 \le d(\vec{q}) < d_c^* \text{ and } \alpha \ge 0 \\ \vec{V}_{des} + \vec{V}_{pb} & \forall \ 0 \le d(\vec{q}) < d_c^* \text{ and } \alpha < 0 \\ \vec{V}_{des} + \vec{V}_s & \forall \ d_c^* \le d(\vec{q}) < d^* \text{ and } \alpha \ge 0 \\ \vec{V}_{des} & \text{otherwise} \end{cases} \qquad (12)$$

where α is the component of $\vec{V}_{des}$ in the direction of $\hat{v}_{pb}$ (Fig. 5). As shown in Fig. 5, summing the pushback and slowdown velocity vectors with the desired velocity vector ($\vec{V}_{des}$) produces a limited velocity command vector ($\vec{V}_{cmd}$). This behavior is defined as such based on feedback from the clinical practitioners as well as ensuring stable performance at or nearing the boundary transitions. After the velocity reductions are applied to the defined regions as outlined in (12), $\vec{V}_{cmd}$, is applied to (8).

The nominal value for the configurable safety distance (d^*) where the slowing of input commands begins is 10 cm from any safety region, and the default value for the configurable critical pushback distance (d_c^*) is 2.5 cm. If the endpoint is
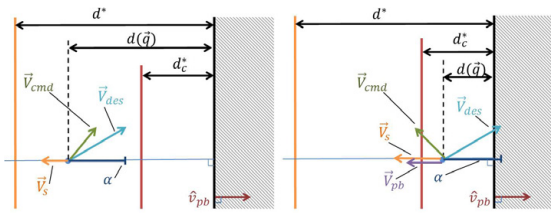
Fig. 5. Depiction of implemented velocity reduction zones within a virtual fixture. Note that the opposing influence on the desired velocity changes as the endpoint position, $d(\vec{q})$, crosses d^* and d_c^*.

Fig. 6. Experimental setup of Vicon tracking of MPL coordinate frames. Vicon-tracked motion is compared to position data of internal sensors.

close to multiple safety regions, the velocity reductions due to each safety region are added together to determine the final commanded velocity.

III. MPL TRACKING AND CALIBRATION

A. Test Apparatus

A series of tests were conducted to evaluate the accuracy of the reported positions from the internal MPL joint sensors, as well as to assess the performance of the proposed safety controls dictated by FRVFs. To externally track and measure the limb position during movement, the MPL was mounted in the center of an in-house Vicon test laboratory consisting of eight Vicon cameras (Vicon, Oxford, UK) with overlapping fields of view (Fig. 6). Four reference markers were placed in a rigid geometry relative to the static MPL shoulder bracket, and plates with fixed Vicon marker locations were mounted to the chassis of the lower arm segment and hand of the MPL. These plates were fixed relative to the respective proximal joints of the limb. Using measurements from the hardware models, marker locations were estimated relative to the body-fixed frame of interest. For example, markers rigidly mounted to the shoulder bracket were measured relative to the MPL shoulder frame (Frame-0 in Fig. 3), and markers rigidly mounted to the hand were measured relative to the endpoint frame (Frame-ep in Fig. 3).

Tracking of these markers permitted the ground-truth measurement of three frames affixed to the MPL (shoulder, forearm, and palm). For comparison to the MPL sensor data, joint angles were also estimated from these measured frames by fitting the kinematic model described in Section II-A and Vicon marker positions estimated from hardware models to the marker positions measured by the Vicon setup. The kinematic model was then fit to the data by minimizing a cost function defined by the summed euclidean distances between modeled and measured marker positions. The minimization was conducted using `fmincon` (MATLAB®, MathWorks, Natick, MA).

These Vicon-based frame and joint measurements were then compared to the endpoint estimates and joint positions determined by the internal MPL sensors in order to validate the capability of the MPL to track its position in real-time. In addition to the Vicon cameras, three video cameras were used during the experimental validation along the X, Y, and Z axes to provide qualitative feedback for MPL trajectory smoothness and jitter and to examine limb movement along a single plane (supplementary video).
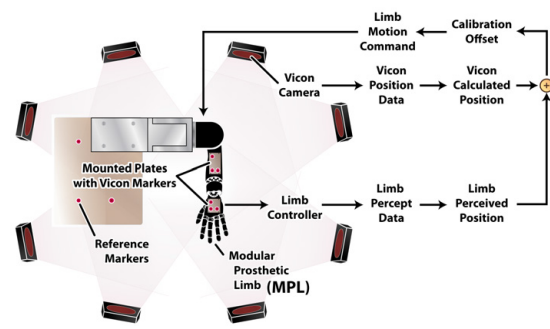
B. Test Setup and MPL Control

During testing, the MPL was controlled using multiple command inputs, which included: 1) a multi-directional joystick (Logitech Gamepad F310, Logitech, Newark, CA) that sent endpoint velocity commands; 2) a teleoperation setup that collected information from a wearable Cyberglove (Cyberglove Systems, San Jose, CA) and Microstrain GX3 inertial sensors strapped to the wrist and elbow (Microstrain, Williston, VT) to construct a joint-angle position command set; and, 3) pre-programmed scripts (MATLAB®, Mathworks, Natick, MA) that sent direct joint angle position commands. For each control paradigm, these software commands were packaged into MPL-UDP messages that were sent to VulcanX. The VulcanX software continually received and logged percepts sent from the MPL that provided position information for each joint. In conjunction with the onboard hardware controllers, VulcanX evaluated the real-time error between the commanded motion intents and the received internal percepts in order to update the limb trajectory and to perform any necessary modifications to restrict motion into any 3-dimensional FRVF regions that were predefined in the VulcanX software configuration file.

C. Test Protocol

For the test series performed, virtual fixtures were defined both in an area representing the head and in a region at the periphery of the limb's reach. This was done to prevent interaction with external fixtures (such as a patient bed or chair) or the surrounding environment.

The first series of tests consisted of the MPL being commanded to move within its allowable workspace and to physically determine the boundaries of operation by reaching the limits of the workspace. The second series measured MPL movement at or near each workspace and FRVF limits to evaluate the accuracy of the tracking plots and their ability to map out defined borders of the workspace. The final series consisted of the MPL attempting to circumvent the set of prohibited areas, and attempt to find possible trajectories that permitted unintended movement into any defined prohibited area. This final series allowed the operator
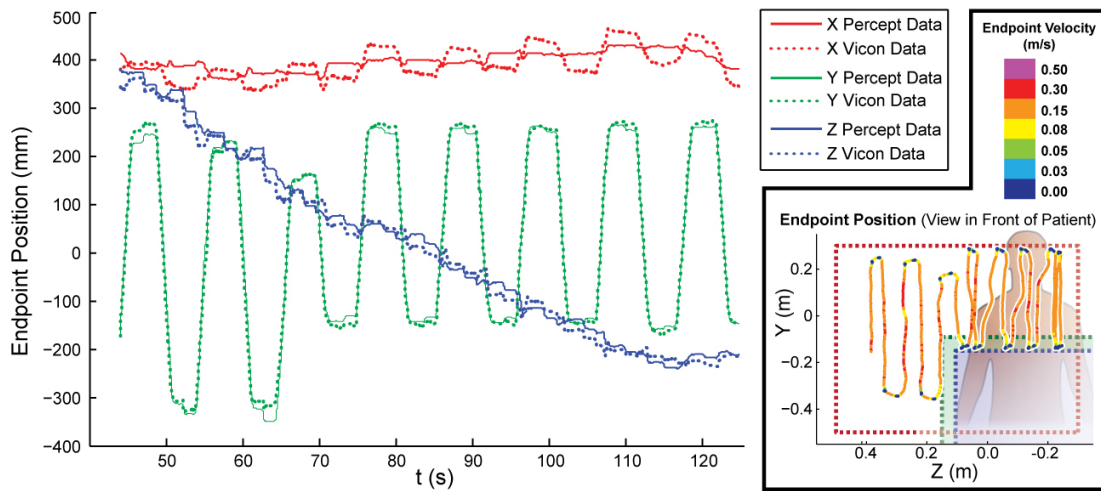
Fig. 7. Time synchronized MPL percepts and Vicon recorded data for testing of the patient virtual fixture in Cartesian space. In this example test, the patient fixture was evaluated and defined for a patient sitting in a wheelchair or lying in a hospital bed.
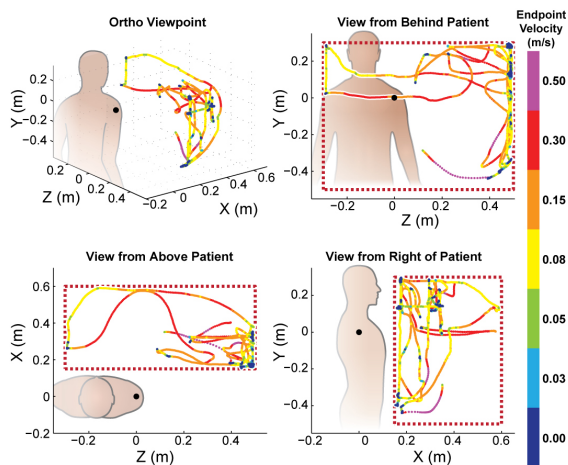
Fig. 8. Percepts data depicting adherence to the workspace virtual fixture based on human joint mapping teleoperation. Here the workspace fixture is defined by the dotted red line.

to evaluate the response to attempted entry into a fixture and comprehensively look for distinct patterns and approaches that may have violated the safety controls in place.

Multiple tests were performed for each series with differing parameters for the MPL's allowable workspace and associated prohibited areas. This methodology was consistent in determining how well the algorithm performed and provided enough data to quantify the test results as successes or failures. The test protocols were executed following verification of the Vicon marker position and visibility.

IV. RESULTS

This testing and data processing evaluated the efficacy of our methods for applying FRVFs to ensure patient safety during clinical self-feeding tests using the MPL. The accuracy of internal MPL position sensors as compared to external motion-tracking data and imposed safety regions were validated by endpoint measurements from motion-

tracking. As this work is directly applicable to multiple clinical collaborations, large efforts were made to provide user-definable safety distances and fixture coordinate definitions. Specifically, the test environment was developed to measure end-effector motion into specific regions of the MPL workspace when these virtual fixtures are imposed. Fig. 4 depicts representative shapes of these restricted regions (both workspace and patient) relative to the total reach of the MPL. The different viewpoints contained in Fig. 8 portray the motion of the internal MPL sensor data (also known as percept data) throughout its workspace adhering to these constraints. As depicted in Fig. 8, there are clear demarcations highlighting the performance of the virtual fixtures. Throughout the test, the user desired velocity was varied (note colored changes according to velocity scale bar) to attempt to use momentum to circumvent the software limits for the fixtures and the distinct regions where the velocity was forced to zero (blue colored areas). Furthermore, the FRVF regions were built for a patient operating the MPL both upright (Fig. 8) and lying down (Fig. 7).

Incorporating the Vicon motion-tracking system was significant and helpful to identify possible inaccuracies in the internal percepts, kinematic errors, or possible miscalibration of joints. As laid out in Fig. 6, the Vicon data was referenced as a "gold standard," and can be integrated in the feedback loop to determine and update the calibration offsets of the limb. Accurately modeling the MPL's kinematics (Fig. 3) and Vicon marker placement was essential in quantifying the movement of the end-effector in 3-D space. When accurately defined and used in the kinematic algorithms, this method resulted in MPL motion that was calibrated and that accurately adhered to the FRVFs.

Fig. 7 compares the Vicon data with percept data for each axis component as the endpoint moves in Cartesian space throughout the trial testing an example patient virtual fixture. Since these fixtures are clinician configurable, they can be adjusted as necessary for a specific clinical application. As
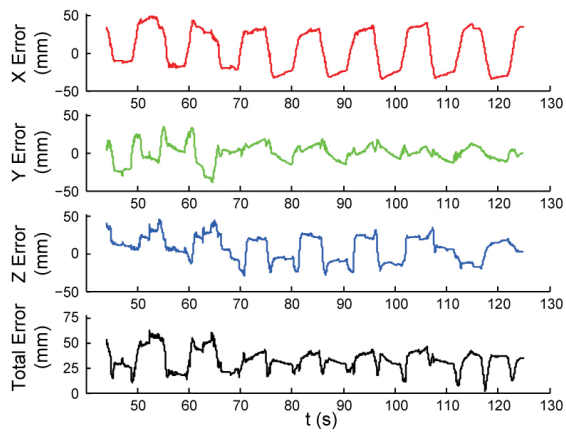
Fig. 9. Error measurement in x, y, z, and Euclidian distance for MPL percepts compared to Vicon collected data as depicted in Fig. 7. The mean value for the lower plot showing Euclidian distance is 3.3 ± 1.0 cm.

indicated in Fig. 7, as the path approaches the patient fixture and reduced velocity zone (dotted green and blue lines in the inset), two things happen. The first is the distance traveled along the y-axis becomes sandwiched between the workspace and the patient fixture, effectively preventing motion into a region that could be occupied by a person. The second is the velocity values when close to these fixtures are noticeably lower ($\sim$0 - 0.03 m/s) than when in open space ($\sim$0.03 - 0.08 m/s) when responding to similar input commands. This is a result of the reduced velocity imposed close to the boundary planes defined by the fixtures. The resultant Euclidean distance error measurement between the Vicon data and MPL percepts is shown in Fig. 9, and reached a one sample maximum of 6.3 cm with a mean value of 3.3 ± 1.0 cm. Individual axis errors are also displayed reflecting a bounded error within approximately 5.0 cm throughout the trial.

V. DISCUSSION

There are sources contributing to the errors illustrated in Fig. 9. The first is the backlash present in the joints of the MPL. Given the development of the MPL as a prosthetic device, weight, size, maximum torque output, and speed (60 Nm for upper arm joints at 120 deg/s) were design constraints favored over reduced/anti-backlash mechanisms used in manipulators intended for precise positioning applications. In this experiment, the percepts data is based upon the closed loop controlled motor rotor position, which doesn't account for backlash at the joints and assumes accurate tracking at the output. Since this geartrain lash is after the very precise hall effect sensors measuring the rotary position of the motor's rotor, it is difficult to detect and counteract. This lash is detected by the sine-cosine encoder, however, controlling for this lash is difficult because it is a function of the MPL's configuration and motion. An additional source of error can come in the form of inaccuracy in joint level calibration; however, steps were taken to minimize this effect, and future work will address rigorous calibration of the MPL using the Vicon system. Despite errors, this testing and algorithm

implementation was able to demonstrate that percept and Vicon system results were well within the required tolerances to ensure patient safety, and percept data clearly shows the MPL in compliance with imposed virtual fixtures allowing for clinical use of the MPL for self-feeding. Accomplishing ADLs such as self-feeding using neural-based control of prosthetic systems such as the MPL is staged to have enormous positive impact in the lives of disabled people. The experimental validation described here was motivated by a quadriplegic patient with implanted intracortical electrodes to feed herself in a method that considered patient safety as paramount.

Our approach attempted to allow for maximum flexibility by the end-user or patient, in determining safety tolerable distances and defining prohibited areas of operation. As the standard endpoint control scheme is fundamentally a rate control algorithm, implementation using an agile software development cycle naturally led to a solution in which opposing velocities could be used to prevent the limb from passing defined virtual fixtures. Internally recorded percept data was validated using a motion-tracking system and shown to be successful in denying the end effector into these areas. Future studies will be necessary to investigate an automated calibration procedure in which iterative assessments of internally-sensed joint positions and motion-tracking data followed by compensatory automated-adjustment of limb parameters can be used to converge the two data sets within a predefined threshold. This methodology would permit rapid prosthetic calibration following hardware repairs, as well as initial setup for newly assembled limb segments.

VI. ACKNOWLEDGMENTS

REFERENCES

[1] J. Donoghue, "Bridging the brain to the world: A perspective on neural interface systems," *Neuron*, vol. 60, no. 3, pp. 511–521, Nov. 2008. [Online]. Available: http://linkinghub.elsevier.com/retrieve/pii/S0896627308008970

[2] A. M. Green and J. F. Kalaska, "Learning to move machines with the mind," *Trends in Neurosciences*, vol. 34, no. 2, pp. 61–75, Feb. 2011. [Online]. Available: http://linkinghub.elsevier.com/retrieve/pii/S0166223610001682

[3] V. Gilja, C. A. Chestek, I. Diester, J. M. Henderson, K. Deisseroth, and K. V. Shenoy, "Challenges and opportunities for next-generation intracortically based neural prostheses," *IEEE Transactions on Biomedical Engineering*, vol. 58, no. 7, pp. 1891–1899, Jul. 2011. [Online]. Available: http://ieeexplore.ieee.org/lpdocs/epic03/wrapper.htm?arnumber=5699350

[4] M. S. Johannes, J. D. Bigelow, J. M. Burck, S. D. Harshbarger, M. V. Kozlowski, and T. Van Doren, "An overview of the developmental process for the modular prosthetic limb," *Johns Hopkins APL Technical Digest*, vol. 30, no. 3, p. 207216, 2011. [Online]. Available: http://www.jhuapl.edu/techdigest/TD/td3003/30_3-Johannes.pdf

[5] A. Harris, K. Katyal, M. Para, and J. Thomas, "Revolutionizing prosthetics software technology," in *2011 Ieee International Conference on Systems, Man, and Cybernetics (smc)*. New York: Ieee, 2011, pp. 2877–2884, WOS:000298615103020.

[6] M. Grebenstein, M. Chalon, W. Friedl, S. Haddadin, T. Wimbock, G. Hirzinger, and R. Siegwart, "The hand of the DLR hand arm system: Designed for interaction," *The International Journal of Robotics Research*, vol. 31, no. 13, pp. 1531–1555, Nov. 2012. [Online]. Available: http://ijr.sagepub.com/cgi/doi/10.1177/0278364912459209

[7] A. D. Ravitz, M. P. McLoughlin, J. D. Beaty, F. V. Tenore, M. S. Johannes, S. A. Swetz, J. B. Helder, K. D. Katyal, M. P. Para, K. M. Fischer, T. C. Gion, and B. A. Wester, "Revolutionizing prosthetics - phase 3," *Johns Hopkins APL Technical Digest*, vol. 31, no. 4, pp. 366–376, 2013.

[8] J. L. Collinger, B. Wodlinger, J. E. Downey, W. Wang, E. C. Tyler-Kabara, D. J. Weber, A. J. C. McMorland, M. Velliste, M. L. Boninger, and A. B. Schwartz, "High-performance neuroprosthetic control by an individual with tetraplegia," *Lancet*, vol. 381, no. 9866, pp. 557–564, Feb. 2013, PMID: 23253623.

[9] "Woman with quadriplegia feeds herself chocolate using mind-controlled robot arm in Pitt/UPMC study." [Online]. Available: http://upmc.com/media/media-kit/bci/Pages/default.aspx

[10] L. B. Rosenberg, "Virtual fixtures: Perceptual tools for telerobotic manipulation," in *Virtual Reality Annual International Symposium, 1993., 1993 IEEE*, 1993, p. 7682. [Online]. Available: http://ieeexplore.ieee.org/xpls/abs_all.jsp?arnumber=380795

[11] L. D. Joly and C. Andriot, "Imposing motion constraints to a force reflecting telerobot through real-time simulation of a virtual mechanism," in *Proceedings of the IEEE International Conference on Robotics and Automation*, ser. IEEE INTERNATIONAL CONFERENCE ON ROBOTICS AND AUTOMATION. NEW YORK: IEEE, 1995, pp. 357–362.

[12] T. Itoh, K. Kosuge, and T. Fukuda, "Human-machine cooperative telemanipulation with motion and force scaling using task-oriented virtual tool dynamics," *Robotics and Automation, IEEE Transactions on*, vol. 16, no. 5, p. 505516, 2000. [Online]. Available: http://ieeexplore.ieee.org/xpls/abs_all.jsp?arnumber=880801

[13] J. Abbott, P. Marayong, and A. Okamura, "Haptic virtual fixtures for robot-assisted manipulation," *Robotics research*, p. 4964, 2007. [Online]. Available: http://www.springerlink.com/index/G4L2XM653U636XT2.pdf

[14] R. J. Anderson and M. W. Spong, "Bilateral control of teleoperators with time delay," *Automatic Control, IEEE Transactions on*, vol. 34, no. 5, p. 494501, 1989. [Online]. Available: http://ieeexplore.ieee.org/xpls/abs_all.jsp?arnumber=24201

[15] G. S. Guthart and J. K. Salisbury Jr, "The intuitive< sup >TM</sup> telesurgery system: overview and application," in *Robotics and Automation, 2000. Proceedings. ICRA'00. IEEE International Conference on*, vol. 1, 2000, p. 618621. [Online]. Available: http://ieeexplore.ieee.org/xpls/abs_all.jsp?arnumber=844121

[16] S. Park, R. Howe, and D. Torchiana, "Virtual fixtures for robotic cardiac surgery," in *Proceedings of the 4th International Conference on Medical Image Computing and Computer-Assisted Intervention*, 2001, p. 14191420. [Online]. Available: http://www.springerlink.com/index/4PPUJK8TKJ6DE2N5.pdf

[17] C. E. Reiley, "Evaluation of augmented reality alternatives to direct force feedback in robot-assisted surgery: Visual force feedback and virtual fixturesEvaluation of augmented reality," Master's thesis, Johns Hopkins University, Apr. 2007.

[18] R. H. Taylor and M. Li, "Optimum robot control for 3D virtual fixture in constrained ENT surgery," in *MEDICAL IMAGE COMPUTING AND COMPUTER-ASSISTED INTERVENTION - MICCAI 2003, PT 1*, ser. LECTURE NOTES IN COMPUTER SCIENCE. BERLIN: SPRINGER-VERLAG BERLIN, 2003, vol. 2878, pp. 165–172.

[19] C. Feng, H. Haniffa, J. Rozenblit, J. Peng, A. J. Hamilton, and M. Salkini, "Surgical training and performance assessment using a motion tracking system," in *Proceedings of European modeling and simulation symposium (EMSS)*, 2006, p. 647652. [Online]. Available: http://www.astec.arizona.edu/sites/astec.arizona.edu/files/pdf_files/MotionTracking%20System.pdf

[20] S. D. Herrell, D. M. Kwartowitz, P. M. Milhoua, and R. L. Galloway, "Toward image guided robotic surgery: System validation," *The Journal of Urology*, vol. 181, no. 2, pp. 783–790, Feb.

2009. [Online]. Available: http://linkinghub.elsevier.com/retrieve/pii/S0022534708027080

[21] S. Payandeh and Z. Stanisic, "On application of virtual fixtures as an aid for telemanipulation and training," in *Haptic Interfaces for Virtual Environment and Teleoperator Systems, 2002. HAPTICS 2002. Proceedings. 10th Symposium on*, 2002, p. 1823. [Online]. Available: http://ieeexplore.ieee.org/xpls/abs_all.jsp?arnumber=998936

[22] J.-C. Latombe, *Robot Motion Planning*. Kluwer Academic Publishers, 1991.